Estimation of surface iron oxide abundance with suppression of grain size and topography effects

Shuho Noda[a] and Yasushi Yamaguchi[b]

[a]Graduate School of Environmental Studies, Nagoya University,
D2-1 (510) Furo-cho, Chikusa-ku, Nagoya, 464-8601 Japan
e-mail: noda-shuho@jogmec.go.jp

Present address:
Metals Exploration Department
Japan Oil, Gas and Metals National Corporation
10-1, Toranomon 2-chome, Minato-ku, Tokyo, 105-0001 Japan

[b]Corresponding author
Graduate School of Environmental Studies, Nagoya University,
D2-1 (510) Furo-cho, Chikusa-ku, Nagoya, 464-8601 Japan
Tel/Fax: +81-52-789-3017
e-mail: yasushi@ nagoya-u.jp

Abstract

Mineral forms of iron oxide, such as hematite, goethite and jarosite, are important because they are widely distributed at the Earth's surface and because they are used as indicators for mineral exploration. Iron oxide abundance in rocks containing these minerals can be estimated from the absorption depth at wavelengths of around 900 nm in a reflectance spectrum, but this depth is also affected by extraneous factors such as grain size and topography. This paper investigated the effect of grain size on reflectance spectra and proposed a method for estimating iron oxide abundance in surface rocks by using remotely sensed data with suppression of the effects of grain size and topography. Reflectance spectra were measured in a laboratory from rock powder samples of different grain sizes containing iron oxide minerals. While the reflectance increased with decreasing grain size, the presence of ferric iron caused the absorption depth to be almost constant at around 900 nm, irrespective of the chemical composition of the sample. In addition, the difference between the reflectance at 550 nm and 760 nm (Slope) was a function of grain size. Iron oxide abundance can be estimated accurately by MCR-900D, which is the maximum absorption depth at the absorption center after the effect of grain size and topography was suppressed by Slope and the continuum-removal method, which takes the ratio between the original spectrum and its continuum, respectively. Correlation of MCR-900D results with datasets of actual spectral and chemical iron oxide laboratory measurements revealed that the mineral forms also need to be considered. MCR-900D results were significantly correlated with rock samples classified as containing different forms of iron oxide minerals (hematite, goethite and jarosite). Finally, MCR-900D was applied to an AVIRIS dataset for the Cuprite site in Nevada, USA. The results represented the enrichment zones of iron oxide within hydrothermally altered areas.

Key words: iron oxide; reflectance spectra; grain size; remote sensing; AVIRIS

1. Introduction

Mineral forms of iron oxide, such as hematite, goethite and jarosite, are widely distributed at the Earth's surface. The presence of ferric iron in these minerals means that they have three diagnostic absorption features in the visible to near-infrared (VNIR) regions; they exhibit charge transfer absorption between 480 and 550 nm, and crystal-field absorption between 630 and 715 nm, and between 850 and 1000 nm (Morris et al., 1985). These spectral features can be used to identify and distinguish between iron oxide minerals. This study considered iron oxide minerals to include hematite (α-Fe_2O_3), goethite (α-FeOOH) and jarosite ($KFe_3(SO_4)_2(OH)_6$). In addition, iron oxide (i.e., ferric oxide or Fe_2O_3) abundance was considered to include iron oxyhydroxide (FeO(OH)) abundance, which is typically measured as Fe_2O_3 in chemical analysis. Most of the studies conducted on these spectral reflectance characteristics to date have been performed in laboratories (Morris et al., 1985; Sherman and Waite, 1985). Studies conducted in the field have shown that iron oxide minerals are not randomly distributed, but that they occur in zones associated with ore deposits (e.g., around ore bodies of porphyry copper deposits) (Townsend, 1987). Consequently, if the distribution of iron oxide minerals is associated with certain ore minerals (Gustafson and Hunt, 1975; Saegart et al., 1974), then locating minerals containing iron oxide can be used to identify sites that may be suitable for mineral exploration (Ciampalini et al., 2013).

In the field of planetary science, remote sensing data has been used to estimate FeO abundance. Iron exists as ferrous oxide on the surface of the moon and as ferric oxide on

71 the Earth. Lucey et al. (1998) estimated the FeO content of areas on the lunar surface after
72 suppressing space weathering effects. On the other hand, the quantitative estimation of
73 ferric iron oxide abundance on the Earth's surface by remote sensing is still in the initial
74 stages. Fe_2O_3 is the most common iron oxide, and its abundance affects the depth for
75 absorption features between 850 and 1000 nm (Cudahy and Ramanaidou, 1992; Hunt and
76 Ashley, 1979). However, since the spectral reflectance of rocks and minerals in remote
77 sensing data is also affected by factors such as chemical composition, topography, mixing
78 and grain size (Murphy and Monteiro, 2013), these factors can affect the absorption depth,
79 which is defined as the difference between the minimum reflectance of an absorption and
80 a reflectance at the same wavelength on the straight line connecting two shoulders on the
81 both sides of an absorption. Given the complexity of the interactions among these factors,
82 their relative contribution to estimates of iron oxide abundance is typically not
83 considered; however, we consider they would amount to several wt%.
84 Previous studies that have attempted to infer iron oxide abundance based on the
85 reflectance spectra of surface rocks and/or rock samples have typically employed band
86 ratios to suppress the effect of topography. For example, Advanced Spaceborne Thermal
87 Emission and Reflection Radiometer (ASTER) band4/band3 is used for estimating iron
88 oxide abundance, and ASTER band2/band1 is used for classifying iron oxide forms
89 (Cudahy, 2012). The band ratio is effective for removing the effect of topography;
90 however, when the slope of the reflectance values of two spectral bands changes due to
91 other effects, such as water content, organic material or grain size, using band ratios is
92 not effective for removing the effect of topography (Murphy and Monteiro, 2013).
93 Although Haest et al. (2012) managed to suppress the contribution of brightness by using
94 reflectance at 1650 nm, which was assumed to be a function of brightness, reflectance at

that wavelength would also be affected by the mineral composition and topography. The continuum-removal method (Clark and Roush, 1984) is a powerful pre-processing procedure that enhances absorptions in reflectance spectra in order to accurately identify minerals, rocks and vegetation (e.g., Gomez et al., 2008; Oshigami et al., 2013; Schmidt et al., 2003). In addition, the method is well suited to identifying minerals and rocks, particularly since the processed spectra are not affected by topography. However, the absorption depth for minerals identified using data processed with the continuum-removal method increases with increasing grain size (Clark, 1999). There are thus no established methods for estimating iron oxide abundance in remote sensing data that can suppress the contribution of grain size and topography.

The primary objective of this study was therefore to develop a method for estimating iron oxide abundance in surface rocks while suppressing the effects of grain size and topography. Accurate estimates of iron oxide abundance are necessary, not only to characterize the geology of an area of interest, but also because iron oxide abundance is used as an indicator of various ore deposits in exploration geology.

Reflectance spectra of samples containing iron oxides were collected, and the relation between grain size and absorption depths at around 900 nm due to iron oxides were investigated in the laboratory. The absorption depth was corrected by the continuum-removal method and the slope of the reflectance spectrum from 550 to 760 nm was plotted to suppress the topography and grain size effect, respectively. The relations between the absorption depths and iron oxide abundance were then established for three iron oxide minerals, and these relations were then applied to actual airborne image data of Cuprite, Nevada, USA obtained by AVIRIS. We discussed the effectiveness of our method for suppressing the grain size and topography effect when estimating iron oxide abundance.

2. Approach

2.1. Absorption depth

The absorption depth for rocks and minerals in this study was obtained by subtracting the continuum of a spectrum from the original spectrum to obtain a normalized absorption depth. The continuum is a convex background that decreases toward the shorter and longer wavelength regions, and can be drawn as a straight line on the reflectance spectra of iron oxide minerals in the region from 760 nm to 1250 nm. Thus, 900D, which is the maximum absorption depth between 850 and 1000 nm, can be calculated using the following equation:

$$900D = 900C - 900R \quad (1)$$

where 900C is a continuum value of a spectrum at approximately 900 nm, and 900R is the original spectral reflectance at around 900 nm. We assumed that the continuum represents the slopes of absorption values centered outside the 900 nm region due to other chemical components. In this way, the continuum-removal method would allow us to examine absorption by iron oxide only centered at around 900 nm.

In order to suppress the effects of grain size and topography, we introduced two absorption depths modified from 900D. CR-900D stands for Continuum-Removed 900D and indicates an absorption depth obtained from the reflectance spectrum after suppression of the topography effect by the continuum-removal method. MCR-900D stands for Modified CR-900D and indicates an absorption depth obtained from the reflectance spectrum after suppression of the effects of grain size and topography by the

143 slope and the continuum-removal methods, respectively. The methods for calculating CR-
144 900D and MCR-900D are explained in the following sections.
145
146 *2.2. Topographic correction*
147 At wavelengths longer than 550 nm, spectral reflectance increases at a constant rate as
148 grain size decreases, but 900D does not change. In other words, differences in the
149 reflectance values of samples with two different grain sizes are constant in this
150 wavelength region. On the other hand, topography changes both spectral reflectance and
151 900D. The spectral reflectance of minerals and rocks is multiplicatively affected by
152 topographic slopes (Green and Craig, 1985). If a the topographic slope is assumed to be
153 ã, then the topography effect is indicated as T(ã) (e.g., $T(ã) = \cos^2 ã$). The apparent
154 reflectance with the topography effect (R*topo*) can be expressed by the following
155 equation:
156
157 $$Rtopo = R \times T(ã) \quad (2)$$
158
159 where R is the original spectral reflectance, and T(ã) affects the spectral reflectance in all
160 wavelength regions at a constant ratio regardless of the material in a pixel.
161 The continuum-removal method of Clark and Roush (1984) can then be applied to
162 suppress the effect of topography. A continuum-removed spectrum can be derived by
163 dividing an original spectrum (R) by its continuum (C), and the absorption depth due to
164 ferric iron can generally be obtained by the following equation:
165
166 $$CR\text{-}900D = 1.0 - 900R / 900C \quad (3)$$

where CR-900D is the absorption depth at an absorption center around 900 nm formed by ferric iron in a continuum-removed spectrum, 900R is the original spectral reflectance at the absorption center of the original spectrum, and 900C is the continuum value of the original spectrum at the absorption center in the wavelength region of 760 nm to 1250 nm. The CR-900D value of 0.0 means that the original reflectance matches its continuum (i.e. the reflectance peak between two absorptive or non-absorptive regions). The CR-900D is not affected by the effect of topography, because both the original spectrum and its continuum change at the same rate T(ã) in equation (2), thus 900R/900C does not change either by the effect of topography.

2.3. Reflectance measurements for defining the grain size effect

Five rock (A, B, E, F, G in Table 1 and Figure 1) and two sand (Sample C, D) samples containing iron oxide minerals were used to investigate spectral changes attributed to different grain sizes. These samples were collected in Utah and Nevada, USA.; four contained hematite, two contained goethite, and one contained jarosite. The sand samples were divided by sieving, and the remaining rock samples were powdered using a ball mill followed by sieving. The sand samples were not powdered, because they consisted of fine quartz grains which were ready for sieving. Grain-size bins for sieving were <25 μm, 25-44 μm, 44-75 μm, 75-125 μm, 125-180 μm, 180-250 μm, and 250-500 μm. Some grain size fractions could not be prepared because of low sample volumes.

Reflectance spectra of each sample with different grain sizes were measured in the laboratory using a spectroradiometer (FieldSpec Pro, ASD Inc., Co) which has 2150 contiguous spectral bands with wavelengths ranging from 350 to 2500 nm, and a spectral

resolution of 3 nm at 700 nm and 30 nm at 1400 and 2100 nm. In this study, reflectance in laboratory measurements refers to the ratio between radiance from a target and radiance from a Lambertian surface under the same measurement conditions. A Spectralon panel (Labsphere Inc., NH) was used as a reference and was assumed to be a Lambertian surface. A halogen lamp was used as an illumination source, but reflectance spectra in the shorter-wavelength region were noisy due to the low light intensity. Therefore, the spectral data for wavelengths shorter than 450 nm were not used in this study. Reflectance spectra of each sample were measured five times, and the reflectance and absorption depth values were averaged. The RMS error of five measurements for each sample was less than 1% of reflectance at wavelengths longer than 450 nm. The chemical compositions of all samples were also analyzed by X-Ray fluorescence (XRF) spectroscopy (ZSK Primus II instrument equipped with a Rh mode, Rigaku, Japan) (Table 1).

Figure 1 shows reflectance spectra obtained for samples of different grain sizes. Changes in reflectance spectra with grain size differ according to whether the minerals being analyzed are transparent, opaque or trans-opaque (Salisbury and Hunt, 1968). As the grain size decreases, the reflectance of transparent minerals (e.g., silicates) increases, while that of opaque minerals (e.g., metal sulfides) decreases. Some iron oxide minerals, such as goethite, hematite, and limonite are trans-opaque minerals, which means that as the grain size decreases, the reflectance of these minerals decreases at wavelengths <550 nm and increases at wavelengths >550 nm (Hunt et al., 1971; Townsend, 1987). As the grain size decreases, the absolute reflectance (brightness) of samples increases at wavelengths >550 nm. On the other hand, the absorption depth at around 900 nm hardly changed due to grain size variation, irrespective of the mineral forms of any iron oxide present.

Spectral and chemical datasets were prepared in order to correlate the absorption depth obtained from reflectance spectra in rocks with iron oxide abundance. A total of 43 rock samples containing iron oxide minerals were used (hematite: 17, goethite: 21 jarosite: 5). Of these, 14 rock samples containing goethite or hematite were selected from the data catalog of Urai et al. (1989), and the rest of the samples were collected in Utah and Nevada, USA. We used these data sets, because the range of Fe_2O_3 contents was much larger than those of the seven powdered samples on Table 1.

The spectral dataset of Urai et al. (1989) consisted of reflectance spectra and chemical and mineral compositions for 111 rock and mineral samples. Reflectance spectra were measured in 800 contiguous spectral bands at wavelengths from 450 to 2600 nm using a spectroradiometer (Infrared Intelligent Spectroradiometer, Geophysical Environment Research, NY). The chemical compositions of the powdered samples were analyzed by inductively coupled plasma - atomic emission spectroscopy (ICP-AES). Reflectance spectra of the samples collected in Utah and Nevada, USA. were measured using a spectroradiometer (FieldSpec pro, ASD Inc., CO) and their chemical compositions were analyzed by XRF (ZSK Primus II instrument equipped with a Rh mode, Rigaku, Japan). The depth of the absorption feature at around 900 nm due to ferric iron was calculated from the reflectance spectra, and this was correlated with the actual Fe_2O_3 content (wt%) in the chemical dataset.

2.4. Grain size regression

To account for the contribution of the grain size when estimating the iron oxide abundance of trans-opaque minerals such as hematite and goethite, the difference between the reflectance values at 550 nm and 760 nm (*Slope*) was used. This relationship can be

239 expressed as:

240

241 $$Slope = 760R - 550R \quad (4)$$

242

243 where 760R and 550R are the reflectances at 760 and 550 nm, respectively; 760R is the
244 reflectance peak between the two absorption features centered at around 660 and 900 nm
245 due to ferric iron. In reflectance spectra of iron oxide minerals with various grain sizes,
246 550R behaves like a fixed point. Previous studies showed that the behavior of the spectral
247 changes of iron oxide minerals due to grain size differs at wavelengths shorter than 550
248 nm and longer than 550 nm (Hunt et al., 1971; Townsend, 1987). Thus, as the grain size
249 of iron oxide minerals increases, *Slope* increases as a function of the grain size (Fig. 2).
250 The effect of the grain size on a reflectance spectrum can therefore be suppressed by
251 subtracting *Slope* from the original spectrum:

252

253 $$\text{Modified-R} = R - Slope \quad (5)$$

254

255 Here, Modified-R is a reflectance spectrum with grain size effect suppressed, and R is the
256 original reflectance spectrum. Modified-R can thus be used to suppress differences in
257 absolute reflectance due to the effect of grain size.

258

259 *2.5. Suppression of grain size and topography effects*

260 The conventional band ratio is an effective method for suppressing the effect of
261 topography, but the ratio of two reflectance values also depends on the original
262 reflectance values. For example, as grain size decreases, the reflectance increases and

consequently, the ratio of the two reflectance values decreases.

$$\{R(\lambda_1) / R(\lambda_2)\}_{\text{large grain}} > \{R(\lambda_1) / R(\lambda_2)\}_{\text{small grain}} \quad (6)$$

where $R(\lambda_i)$ is the reflectance at wavelength λ_1.

Therefore, to suppress the effects of grain size and topography, it is necessary to remove the effect of grain size prior to removal of the effect of topography by a multiplicative operation (Fig. 3), as doing so will suppress changes in absolute reflectance due to grain size.

To suppress the effects of grain size and topography, the continuum-removal method must be applied to Modified-R. Thus, MCR-900D, which is the absorption depth at which both effects are suppressed, can be obtained by the following equation:

$$\text{MCR-900D} = 1.0 - \text{M900R} / \text{M900C} \quad (7)$$

Here, M900R and M900C are the spectral reflectance and its continuum at an absorption center at which reflectance is the local minimum, respectively, derived from Modified-R. An absorption center at around 900 nm is extracted in advance from the original reflectance spectrum, because the continuum-removal method often changes the wavelength of the absorption center (Haest et al., 2012). MCR-900D can be used to effectively estimate iron oxide abundance (wt%) using spectral data, as effects of grain size and topography suppressed.

2.6. Application to AVIRIS

2.6.1. Study area

The study area selected to evaluate the proposed method for estimating iron oxide abundance was the Cuprite area in Nevada, USA, approximately 200 km northwest of Las Vegas (the center of Fig. 5; N37.53, W117.18). The area has been selected by geological remote sensing studies to evaluate new instruments and methods because of the dry conditions, minimal vegetation, and abundance of clay and iron oxide minerals due to extensive hydrothermal alteration (e.g., Clark et al., 2006; Swayze et al., 2014; Yamaguchi and Naito, 2003). Hydrothermal alteration occurred as a result of interaction between rocks and hot water, which was heated by magmatic activity in the mid- to late Miocene (Ashley and Abrams, 1980). The area is divided into two subregions by Highway 95, which bisects the study area along a north-south axis. In the western region, Cambrian metasedimentary rocks, Paleogene conglomerate, and intrusive rocks that were hydrothermally altered dominate, while in the east, Paleogene rhyolitic ash-flow tuff, conglomerate, and basalt are distributed. Vegetation cover in this area is a few percent and we assumed that vegetation did not markedly affect the spectral reflectance of the AVIRIS data.

2.6.2. Image data

The proposed method for estimating the iron oxide abundance was applied to Airborne Visible/Infrared Imaging Spectrometer (AVIRIS) image data. AVIRIS is a hyperspectral sensor that has 224 contiguous spectral bands with wavelengths ranging from around 400 to 2500 nm and a spectral resolution ranging from 14 to 23 nm (Green et al., 1998). AVIRIS is well suited to a wide variety of fields, including geology, environmental studies, agriculture, and oceanography. The AVIRIS data for the Cuprite area was

obtained from the NASA website (http://aviris.jpl.nasa.gov/data/free_data.html). The spatial resolution of the image is 17 m and the target area is about 8.7 km from east to west and 10.4 km from north to south. We used the AVIRIS Standard Data Product of Cuprite, which was converted to surface reflectance. We assumed that the atmospheric correction was included in the reflectance conversion processing by NASA.

2.6.3 Data processing

The hydrothermally altered areas were also divided into silicified, opalized, and argillized zones based on the degree of alteration (Ashley and Abrams, 1980). The silicified zone consists mainly of quartz and chalcedony, the opalized zone has alunite and kaolinite deposits, and the argillized zone has kaolinite deposits (Swayze et al., 2014). A supervised classification of AVIRIS VNIR data (400-1350 nm) was conducted in order to comprehend the distribution of various iron oxide minerals and to select an appropriate linear regression for each pixel.

Iron oxide abundance in the Cuprite area was estimated using AVIRIS data after calculating the absorption depth by MCR-900D. Absolute values of the iron oxide abundance for each pixel were determined using the three linear regressions corresponding to the different mineral forms of iron oxide.

3. Results

3.1. Verification of spectral measurement results

The average difference between the maximum and minimum values of 900D in the reflectance spectra of seven different grain size samples was less than 0.01% (reflectance value). We can therefore conclude that the absorption depth is almost constant even if the

grain size changes. In previous studies, the absorption depth at around 900 nm of goethite and hematite increased as the grain size decreased (Hunt et al, 1971), while the absorption depth at around 1000 nm of the other minerals such as amphibole and olivine became shallower as the grain size decreased (Hunt and Salisbury, 1970); however, such a trend was not apparent in our measurement results. In addition, the differences among the reflectance spectra of different grain size samples were almost constant (less than 1% reflectance difference), which means that neither the shape of the spectra nor 900D changed, and that grain size has an additive effect on reflectance spectra. There were differences between our measurements and the measurements by Hunt and Salisbury (1970) and Hunt et al. (1971). For example, we used rock powder samples containing iron oxides, while Hunt and Salisbury (1970) and Hunt et al. (1971) used powders of pure minerals. Moreover, we measured samples measuring 25 to 500 μm, while the measurements of Hunt and Salisbury (1970) and Hunt et al. (1971) used very fine grain samples (0-5 and 0-74 μm). In addition, the absorption depths due to OH molecular vibrations at around 1420 nm, 1920 nm and 2200 nm did not change markedly for different grain sizes.

The reason why reflectance increases while the spectral shape and absorption depth remain relatively constant as the grain size decreases is probably due to the increase in the amount of first surface reflection and multiple scattering (Cooper and Mustard, 1999). Surface scattering is dominant in the VNIR regions, while volume scattering is dominant in the thermal infrared region. The reflectance from a single grain is generally determined by boundary reflection (first surface reflection), internal reflection, effective grain size, and the absorption coefficient (Hiroi and Pieters, 1992). These reflections are not affected by wavelength because the grain sizes examined in this study are larger than the

359 wavelengths of VNIR light. In addition, since surface backscattering increases as grain
360 size decreases, reflectance increases independently of wavelength. On the other hand,
361 previous studies demonstrated an increase in absorption depth with decreasing grain size
362 until the absorption path length coincided with the mean optical path length (Hapke,
363 1993). The absorption depth at around 600 nm decreased with decreasing grain size
364 because volume scattering played a smaller role compared to first surface scattering.
365 However, at around 900 nm, the absorption depths were almost constant in this study. It
366 is considered that the absorption coefficient did not change markedly with grain size,
367 because larger grains might consist of aggregations of finer grains in the actual rock and
368 sand samples. It should be noted that grain shape also plays an important role in the
369 effective grain size and in changes in the scattering intensity (Hiroi and Pieters, 1992).
370
371 *3.2. Correlation between absorption depth and iron oxide abundance*
372 The depth due to ferric iron at the absorption center derived using MCR-900D was
373 correlated with the actual Fe_2O_3 content in the spectral and chemical datasets of the 43
374 rock samples to estimate surface iron oxide abundance in remotely sensed image data.
375 MCR-900D was positively correlated with Fe_2O_3 content ($R^2 = 0.49$) with a root mean
376 squared error (RMSE) of 3.57 wt% using a linear regression for all the iron oxide samples.
377 The variation in the mineral forms of iron oxide caused differences in the brightness,
378 shape, and position of absorption centers in their reflectance spectra in the VNIR region.
379 For example, the absorption center in the reflectance spectra of hematite, goethite and
380 jarosite is around 850 nm, 940 nm and 900 nm (Hunt and Ashley, 1979).
381 Figure 4 shows the correlations between MCR-900D and Fe_2O_3 content for the
382 different mineral forms of iron oxide with significantly higher correlation coefficients

(hematite: $R^2 = 0.75$, goethite: $R^2 = 0.82$, jarosite: $R^2 = 0.94$). Moreover, RMSEs obtained using linear regression were highly improved for each mineral form (hematite: 0.82 wt%, goethite: 2.59 wt%, jarosite: 0.31 wt%). The major reason for the deviations from the regression lines was likely due to the different compositions of the various minerals in the samples which may have caused different multiple reflections. After classifying the mineral forms of iron oxide using the wavelengths of the absorption center, iron oxide abundance was estimated by image processing using the following three linear regressions (hematite: $y = 5.63x - 0.02$, goethite: $y = 25.82x - 1.13$, jarosite: $y = 20.84x - 2.27$; where MCR-900D is substituted for x and y is iron oxide abundance). In this study, each pixel was classified according to the wavelength of absorption center; <900 nm to hematite, 900 - 930 nm to jarosite, and >930 nm to goethite (Fig. 3).

3.3. AVIRIS data analysis

The supervised classification result (Fig. 5) showed that iron oxide minerals were correlated with the opalized and argillized zones. Moreover, the mineral forms of iron oxide differed between the western and eastern regions. Jarosite and jarosite + goethite are common in the western region, while hematite is locally distributed in the eastern region and to the north of the silicified zone. Visually, the color of the surface rocks including iron oxide minerals is yellowish in the western region and red in the eastern region. Differences in the distribution of iron oxides probably depend on the depth of erosion and it is suggested that the western region is more eroded than the eastern region.

In the iron oxide abundance image (Fig. 6), regions with larger absorption depths at around 900 nm in the hydrothermally altered areas were well represented by all three methods. The highest level of iron oxide abundance was approximately 6 wt%, and such

areas were distributed mainly in the western hills of the Cuprite area (shown as red in Fig. 6). As can be seen from iron oxide abundance map and the mineral distribution map (Fig. 5), in terms of iron oxide abundance, the distribution of hematite (ca. 2 wt%) in the eastern area was relatively low compared to that in the western area, because the slope of the regression line in hematite samples was smaller than those of jarosite and goethite (Fig. 4). It is suggested that rocks with hematite appear reddish, even if iron oxide abundance is low. In addition, though iron oxide was not extracted from the silicified zone, the enrichment zones were consistent with the opalized and argillized zones. Enrichment zones consisting of iron oxide with jarosite and goethite are important in exploration geology settings.

3.4. Validation of AVIRIS results

Although the results obtained using AVIRIS data processed by these three methods (MCR-900D, CR-900D, and 900D) were generally similar (Fig. 7), the results obtained by MCR-900D showed a strong contrast between the altered and non-altered areas. Southwest of the hills in the western region, absorption depth estimated by CR-900D was larger than that estimated by the other methods because the reflectance was lower than the altered areas in the hills. Conversely, reflectance was lower in the areas with high levels of hematite in the eastern hills. In addition, iron oxide abundance estimated by 900D and CR-900D in the hills to the west and southwest of the western region was higher than that estimated by MCR-900D. It is therefore necessary to analyze the chemical compositions in the surface rocks in these regions in order to verify the abundance maps.

To investigate whether the effect of topography was suppressed by the processing methods, the average reflectance for all spectral bands was correlated with 900D and

MCR-900D, respectively. It was considered that 900D would essentially only reflect the iron oxide abundance, and that 900D would be independent of the average reflectance. In other words, if the correlation between the average reflectance was weak, then we could assume that the effect of topography was suppressed. However, our results showed that the average reflectance for all bands decreased as the topography effect increased (i.e., an increase in the topographic slope), and the values obtained by 900D decreased accordingly. By being affected by topography, 900D is considered to be dependent on the average reflectance for all bands, implying that iron oxide abundance would be correlated with the average reflectance for all bands.

The coefficients of determination (R^2) between the average reflectance obtained for all AVIRIS bands and 900D and MCR-900D for the Cuprite area were 0.47 and 0.28, respectively; 900D and average reflectance showed a higher correlation compared to MCR-900D, indicating that 900D did not suppress the effect of topography. However, MCR-900D and average reflectance were less strongly correlated, which means that MCR-900D is not affected by topography, likely due to the continuum-removal method. MCR-900D is thus effective for estimating iron oxide abundance by using reflectance spectra in remotely sensed data, as it suppresses the effects of grain size and topography.

4. Discussion

Generally, the SiO_2 content of rocks is inversely proportional to the Fe_2O_3 content. SiO_2-rich rock samples contain higher amounts of transparent minerals such as quartz, and the high reflectance associated with SiO_2-rich sediments is strongly affected by these minerals. Consequently, the increase in the optical depth attributed to these transparent minerals results in overestimates of Fe_2O_3 abundance in Fe_2O_3-poor and SiO_2-rich

455 samples (Haest et al., 2012). Though SiO_2-rich samples contain lower amounts of Fe_2O_3,
456 no such trend was observed in this study. In addition, aluminum substitution in hematite
457 and goethite brings about a shift in the absorption center due to ferric iron at around 900
458 nm toward a longer wavelength (Buckingham and Sommer, 1983; Sommer and
459 Buckingham, 1981). However, since the Al_2O_3 content in rock samples did not affect the
460 absorption depth of iron oxide in this study, it is considered that the presence of other
461 chemicals and their abundances did not alter the absorption depth of ferric iron.

462 Another factor that might affect the correlation between MCR-900D and Fe_2O_3
463 content is the difference between the spectral measurements and chemical analysis of
464 each sample. In the dataset of Urai et al. (1989), the reflectance spectra were measured
465 using the natural surface of samples without any processing. Consequently, mineral and
466 chemical compositions are restricted to the surface of samples. On the other hand, for the
467 chemical analysis in this study, each sample was crushed and powdered, which means the
468 results of the chemical analysis reflected the bulk chemical composition of a sample, i.e.,
469 not only the surface of the sample but also its internal composition. It is therefore likely
470 that the variation observed between the absorption depth and the Fe_2O_3 content occurred
471 due to the difference of the measured materials.

472 The 900D data obtained for the different mineral forms of iron oxide were positively
473 correlated with Fe_2O_3 content (hematite: $R^2 = 0.46$, goethite: $R^2 = 0.39$, jarosite: $R^2 =$
474 0.87). In addition, the RMSE obtained from the linear regression was 1.20 wt% in the
475 hematite samples, 4.70 wt% in goethite samples, and 0.47 wt% in jarosite samples. Thus,
476 MCR-900D was more strongly correlated with iron oxide abundance. The improvement
477 in the correlation observed between MCR-900D and Fe_2O_3 content, compared with 900D
478 and Fe_2O_3 content, was due to enhancement or exaggeration of the absorption feature at

around 900 nm by the continuum-removal method. In addition, these spectral data were all measured in the laboratory, and it is considered that in the field, satellite or aircraft imagery processed with 900D would be more affected by topography compared to MCR-900D, because 900D would be affected by the topography effect as well as noise in actual sensor measurements.

Significantly high correlations were observed between CR-900D and the different mineral forms of Fe_2O_3 in the samples (hematite: $R^2 = 0.71$, goethite: $R^2 = 0.75$, jarosite: $R^2 = 0.94$). Also, the RMSE obtained by linear regression was 0.88 wt% in the hematite samples, 3.07 wt% in the goethite samples, and 0.32 wt% in the jarosite samples. Compared to CR-900D, MCR-900D showed improved correlations in the estimation of iron oxide abundance. As CR-900D is not affected by the effect of topography, we attributed the improvement observed using MCR-900D to suppression of the effect of grain size (the variation of absolute reflectance), obtained by subtracting *Slope* from the spectral reflectance before continuum-removal processing. In jarosite samples, the absence of grain size variation meant that the correlations obtained with MCR-900D did not show any improvement compared to CR-900D, because the grain size of all jarosite samples was 180-500 nm. The correlation between CR-900D and average reflectance in the visible wavelength region ($R^2 = 0.52$) was stronger than that between MCR-900D and average reflectance ($R^2 = 0.39$). This means that CR-900D is still affected by the absolute reflectance at the absorption center, which is affected by chemical and mineral composition as well as grain size variation, because the continuum-removed spectrum is derived from the ratio between the original spectrum and its continuum. Consequently, CR-900D is lower for rocks compared to material with a smaller grain size and higher reflectance.

503 Compared to CR-900D, the difference in estimates of iron oxide abundance obtained
504 by MCR-900D, which is an estimate of the difference between the estimated maximum
505 and minimum abundance values in reflectance spectra obtained for different gain size
506 samples was smaller. However, some samples did not show an improvement in
507 suppression of grain size effect by MCR-900D. The potential effectiveness of MCR-900D
508 is based upon the assumptions that *Slope* increases linearly as grain size decreases, and
509 that reflectance at 550 nm is independent of variations in grain size. If these conditions
510 are not met, then MCR-900D cannot suppress the effect of grain size effectively. On the
511 other hand, the difference in estimates of iron oxide abundance by CR-900D might be
512 larger if the range of grain sizes increases beyond the range examined in this study (<25-
513 500 μm).
514 In comparisons among 900D, CR-900D and MCR-900D, the most accurate estimation
515 of iron oxide abundance on rock surfaces was obtained by MCR-900D, which suppressed
516 the effects of grain size and topography. However, it should be noted that MCR-900D
517 (*Slope*) is dependent upon the spectral properties of trans-opaque minerals, that is, iron
518 oxide minerals. MCR-900D is thus not suitable for estimating the abundance of other
519 chemicals/minerals on rock surfaces with transparent or opaque minerals, such as those
520 with clay minerals at around 2200 nm.
521
522 **5. Summary and Conclusions**
523 The authors developed a new method, called MCR-900D, for estimating iron oxide
524 abundance in rocks containing iron oxide minerals. The method is capable of suppressing
525 the effects of grain size and topography in estimates of iron oxide abundance, which is
526 related to the depth of absorption features conferred by the presence of ferric iron at

around 900 nm (900D).

First, to clarify the effect of grain size on reflectance spectra of rock samples containing iron oxide minerals, spectra were measured in samples of different grain sizes (<25 μm, 25-45 μm, 45-75 μm, 75-125 μm, 125-180 μm, 180-250 μm, and 250-500 μm) using a spectroradiometer. The effects of grain size were:

(1) The spectral reflectance increased as the grain size decreased regardless of the chemical/mineral compositions at wavelengths longer than 550 nm.

(2) The shape and the absorption depth for ferric iron absorption spectra were almost constant.

(3) The difference between reflectance at 550 nm and 760 nm in rocks containing iron oxide minerals (*Slope*) was a function of grain size.

These characteristics were considered in developing MCR-900D in order to suppress the effect of grain size.

On the other hand, since the spectral reflectance of minerals and rocks is multiplicatively affected by topographic slope, the continuum-removal method was employed in pre-processing to suppress the topography effect as well as enhance the absorption features. In order to suppress the effects of grain size and topography, the effect of grain size needed to be removed by a subtractive operation prior to removal of the effect of topography using a multiplicative operation. By performing *Slope* and then continuum-removal processing in turn, MCR-900D can be used to estimate the absorption depth while suppressing the effects of grain size and topography.

MCR-900D was then applied to samples in spectral and chemical datasets with known Fe_2O_3 contents. Analysis of 43 rock samples revealed the following:

(1) The mineral forms of samples need to be considered when extracting spectral

information about the wavelength of the absorption center as well as the absorption depth. The correlations between MCR-900D and the Fe_2O_3 content were significantly improved (all samples: $R^2 = 0.49$, hematite: $R^2 = 0.75$, goethite: $R^2 = 0.82$, jarosite: $R^2 = 0.94$).

(2) The presence of other chemicals, such as SiO_2, did not affect the correlation between MCR-900D and the actual Fe_2O_3 content.

(3) The results of processing using only the continuum-removal method depended on the original absolute reflectance, which meant that the grain size effect cannot be suppressed when using the continuum-removal method alone.

Finally, MCR-900D was applied to the AVIRIS data for the Cuprite area in Nevada, USA. The absorption depth and iron oxide abundance map using linear regression well represented the geology, particularly the distributions of the hydrothermally altered areas. Assuming from the correlations with the average reflectance for all bands, it was concluded that MCR-900D successfully suppressed the topography effect. MCR-900D is thus a simple and effective method for estimating the iron oxide abundance in rocks that can provide valuable information on hydrothermal alteration as well as exploration of ore deposits.

Acknowledgments

We thank Dr. Yoshihiro Asahara of Nagoya University for his assistance with laboratory sieving and XRF analysis, and to Dr. Minoru Urai of the National Institute of Advanced Industrial Science and Technology (AIST) for providing the spectral and chemical datasets. We are grateful to Prof. Alan Gillespie of the University of Washington

and an anonymous reviewer for their constructive comments on this manuscript. We also thank NASA for providing the AVIRIS data of the Cuprite region. This work was supported by JSPS KAKENHI (Grant No. 15H04225).

REFERENCES

Ashley, R. P., & Abrams, M. J., 1980, Alteration mapping using multispectral images-Cuprite mining district, Esmeralda County, Nevada: U. S. Geological Survey Open File Report 80-367, 17p.

Buckingham, W. F., & Sommer, S. E., 1983, Mineralogical characterization of rock surfaces formed by hydrothermal alteration and weathering-Application to remote sensing, Economic Geology, 78, 664-674.

Ciampalini, A., Garfagnoli, F., Del Ventisette, C., & Moretti, S., 2013, Potential use of remote sensing techniques for exploration of iron deposits in Western Sahara and Southwest of Algeria, Natural Resources Research, 22, 179-190.Clark, R. N., 1999, Chapter 1: Spectroscopy of rocks and minerals, and principles of spectroscopy, in Manual of Remote Sensing, Remote Sensing for the Earth Sciences, 3, p. 3-58.

Clark, R. N., & Roush, T. L., 1984, Reflectance spectroscopy: Quantitative analysis techniques for remote sensing applications, Journal of Geophysical Research, 89(B7), 6329-6340.

Clark, R. N., Boardman, J., Brown, J. M., Kruse, F., Ong, C., Brown, C. P. & Swayze, G. A., (2006) Mineral mapping and applications of imaging spectroscopy, Geoscience and Remote Sensing Symposium, IGRASS 2006, IEEE International Conference on IEEE,

599 p.1986-1989.
600 Cooper, C. D., & Mustard, J. F., 1999, Effects of very fine particle size on reflectance
601 spectra of smectite and palagonitic soil, Icarus, 142, 557-570.
602 Cudahy, T., 2012. Satellite ASTER geoscience product notes for Australia, ver. 1, CSIRO,
603 EP-30-07-12-44
604 Cudahy, T., & Ramanaidou, E. R., 1992, Relationships between spectral properties and
605 ferric oxides, CSIRO/AMIRA Project P243, Wembley, Australia, CSIRO Division of
606 Exploration Geoscience Report 244R, 68.
607 Gomez, C., Lagacherie, P., & Coulouma, G., 2008, Continuum removal versus PLSR
608 method for clay and calcium carbonate content estimation from laboratory and airborne
609 hyperspectral measurements, Geoderma, 148, 141-148.
610 Green, A. A., & Craig, M. D., 1985, Analysis of aircraft spectrometer data with
611 logarithmic residuals, Proceedings of Airborne Imaging Spectrometer Workshop, Jet
612 Propulsion Laboratory Publication 85-41, 111-119.
613 Green, O. R., Eastwood, M. L., Sarture, C. M., Chrien, T. G., Aronsson, M., Chippendale,
614 B. J., Faust, J. A., Pavri, B. E., Chovit, C. J., Solis, M., Olah, M. R., & Williams, O.,
615 1998, Imaging spectroscopy and the Airborne Visible/Infrared Imaging Spectrometer
616 (AVIRIS), Remote Sensing of Environment, 65, 227-248.
617 Gustafson, L. B., & Hunt, J. P., 1975, The porphyry copper deposit at El Salvador, Chile,
618 Economic Geology, 70, 857-912.
619 Haest, M., Cudahy, T., Laukamp, C., & Gregory, S., 2012, Quantitative mineralogy from
620 infrared spectroscopic data. I. Validation of mineral abundance and composition scripts
621 at the Rocklea Channel Iron Deposit in Western Australia, Economic Geology, 107,
622 209-225.

623 Hapke, B., 1993, Theory of reflectance and emittance spectroscopy, Cambridge Univ.
624 Press, Cambridge.
625 Hiroi, T, & Pieters, C. M., 1992, Effects of grain size and shape in modeling reflectance
626 spectra of mineral mixtures, Proceedings of Lunar and Planetary Science, 22, 313-325.
627 Hunt, G. R. and Salisbury, J. W., 1970, Visible and near-infrared spectra of minerals and
628 rocks: I. Silicate minerals, Modern Geology, 1, 283-300.
629 Hunt, G. R., Salisbury, J. W., & Lenhoff, C. J., 1971, Visible and near-infrared spectra of
630 minerals and rocks: III. Oxides and hydroxides, Modern Geology, 2, 195-205.
631 Hunt, G. R., & Ashley, R. P., 1979, Spectra of altered rocks in the visible and near infrared,
632 Economic Geology, 74, 1613-1629.
633 Lucey, P. G., Blewett, D. T., & Hawke, B. R., 1998, Mapping the FeO and TiO_2content
634 of the lunar surface with multispectral imagery, Journal of Geophysical Research,
635 103(E2), 3679-3699.
636 Morris, R. V., Lauer, H. V., Lawson, C. A., Girson, E. K., Nace, G. A., & Stewart, C.,
637 1985, Spectral and other physicochemical properties of submicron powders of hematite
638 (á-Fe_2O_3), maghemite (ã-Fe_2O_3), magnetite (Fe_3O_4), goethite (á-FeOOH), and
639 lepidocrocite (ã-FeOOH), Journal of Geophysical Research, 90(B4), 3126-3144.
640 Murphy, R.J., & Monteiro, S. T., 2013, Mapping the distribution of ferric iron minerals
641 on a vertical mine face using derivative analysis of hyperspectral imagery (430-970
642 nm), ISPRS Journal of Photogrammetry and Remote Sensing, 75, 29-39.
643 Oshigami, S., Yamaguchi, Y., Uezato, T., Momose, A., Arvelyna, Y., Kawakami, Y.,
644 Yajima, T., Miyatake, S., & Nguno, A., 2013, Mineralogical mapping of southern
645 Namibia by application of continuum-removal MSAM method to the HyMap data,
646 International Journal of Remote Sensing, 34(15), 5282-5295.

647 Saegart, W, E., Sell, J. D., & Kilpatrick, B. E., 1974, Geology and mineralization of La
648 Caridad porphyry copper deposit, Sonora, Mexico, Economic Geology, 69, 1060-1077.
649 Salisbury, W. E., & Hunt, G.R., 1968, Martian surface materials-Effect of particle size
650 on spectral behavior, Science, 161, 365-366.
651 Schmidt, K. S., & Skidmore, A. K., 2003, Spectral discrimination of vegetation types in
652 coastal wetland, Remote sensing of Environment, 85, 92-108.
653 Sherman, D. M., & Waite, T. D., 1985, Electronic spectra of Fe^{3+} oxides and oxide
654 hydroxides in the near IR to near UV, American Mineralogist, 70, 1262-1269.
655 Sommer, S. E., & Buckingham, W.F., 1981, The role of geological surfaces in
656 determining visible and near infrared signatures, paper presented at the International
657 Geoscience and Remote Sensing Symposium, June 8-10.
658 Swayze, G. A., Clark, R. N., Goetz, A. F. H., Livo, K. E., Breit, G. N., Kruse, F. A.,
659 Stutley, S. J., Snee, L. W., Lowers, H. A., Post, J. L., Stoffregen, R. E., & Ashley, R.
660 P., 2014, Mapping advanced argillic alteration at Cuprite, Nevada using imaging
661 spectroscopy, Economic Geology, 109(5), p. 1179-1221.
662 Townsend, T. E., 1987, Discrimination of iron alternation minerals in visible and near-
663 infrared reflectance data, Journal of Geophysical Research, 92(B2), 1441-1454.
664 Urai, M., Sato, I., Ninomiya, R., Miyazaki, Y., & Yamaguchi, Y., 1989, Reflectance
665 spectra catalog of rocks and minerals in the visible to short-wavelength-infrared region
666 (First volume), pp.367, Geological Survey of Japan, Tsukuba, Japan (in Japanese).
667 Yamaguchi, Y. & Naito, C., (2003) Spectral indices for lithologic discrimination and
668 mapping by using the ASTER SWIR bands, International Journal of Remote Sensing,
669 24(22), p.4311-4323.
670

671 Captions of Table and Figures

672

673 Table. 1 Forms of iron oxide minerals and major chemical compositions of rock (A, B, E,
674 F, G) and sand (C, D) samples used to investigate the grain-size effect.

675

676 Figure 1. Reflectance spectra of the different grain size samples (light blue: <25 μm,
677 blue: 25-45 μm, green: 45-75 μm, orange: 75-125 μm, red: 125-180 μm, brown: 180-
678 250 μm, black: 250-500 μm).

679

680 Figure 2. *Slope* in reflectance spectra of different grain size samples. *Slope* decreases as
681 grain size increases.

682

683 Figure 3. Processing sequence of the proposed method for different forms of iron oxide
684 minerals.

685

686 Figure 4. Correlations between MCR-900D and Fe_2O_3 contents of (a) hematite (n=17),
687 (b) goethite (n=21) and (c) jarosite (n=5) samples.

688

689 Figure 5. Iron oxide mineral map derived from the AVIRIS VNIR (400-1350 nm) data
690 by using the supervised maximum likelihood classifier for the area of hydrothermal
691 alteration at Cuprite in Nevada, USA.

692

693 Figure 6. Iron oxide abundance map derived using MCR-900D for the Cuprite area in
694 Nevada, USA.

695

696 Figure 7. Iron oxide abundance map derived using each method (left: MCR-900D,

697 middle: CR-900D, right: 900D) for the western hills in the Cuprite area in Nevada,

698 USA.

699

700 Table. 1 Forms of iron oxide minerals and major chemical compositions of rock (A, B, E,

701 F, G) and sand (C, D) samples used to investigate the grain-size effect.

Sample	Form	SiO_2 wt%	Al_2O_3 wt%	Fe_2O_3 wt%	CaO wt%	MgO wt%	Na_2O wt%	K_2O wt%	LOI wt%	Total wt%
A	hematite	73.20	12.30	3.73	0.55	0.50	1.08	5.02	4.50	100.88
B	hematite	75.90	10.95	3.84	1.36	0.19	0.08	0.15	7.68	100.15
C	hematite	82.69	5.61	1.01	0.69	0.98	0.79	2.09	2.86	96.72
D	hematite	96.63	0.57	0.06	0.00	0.04	0.00	0.32	0.40	98.01
E	goethite	85.90	1.98	8.10	0.10	0.07	0.04	0.16	2.28	98.63
F	goethite	74.00	12.85	4.03	0.14	0.26	0.38	1.91	8.05	101.62
G	jarosite	37.10	22.00	3.59	0.37	0.05	1.05	4.52	28.10	96.78

702

703

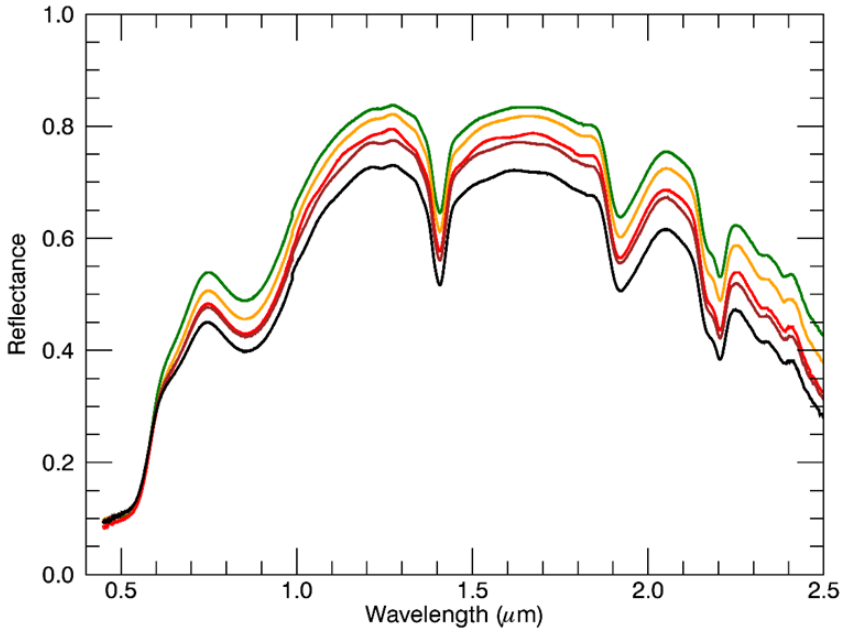

704

705 (a) Sample B

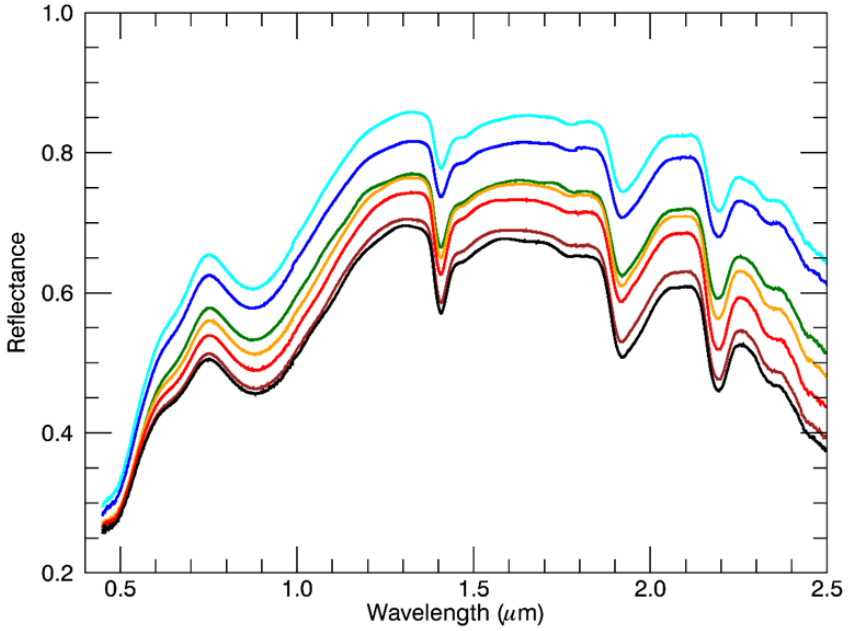

706

707 (b) Sample F

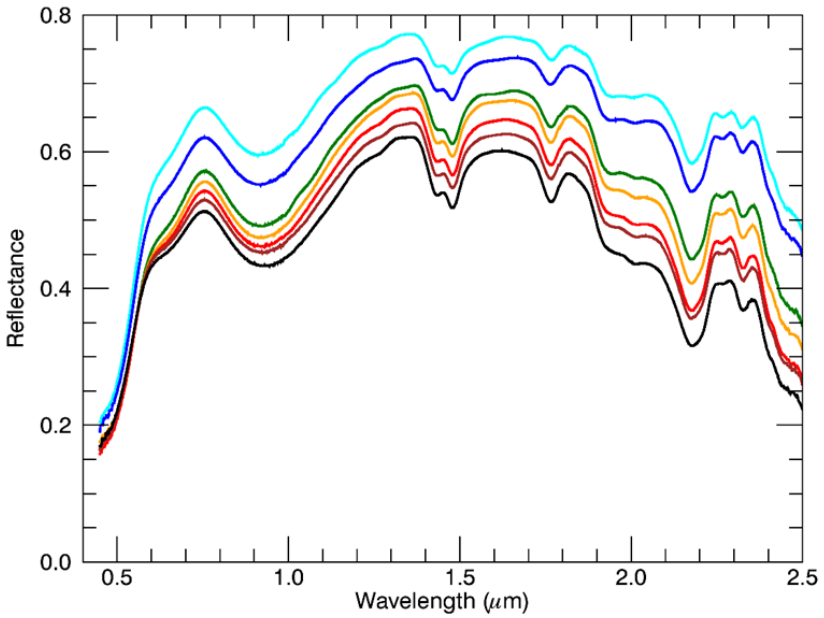

(c) Sample G

Figure 1. Reflectance spectra of the different grain size samples (light blue: <25 μm, blue: 25-45 μm, green: 45-75 μm, orange: 75-125 μm, red: 125-180 μm, brown: 180-250 μm, black: 250-500 μm).

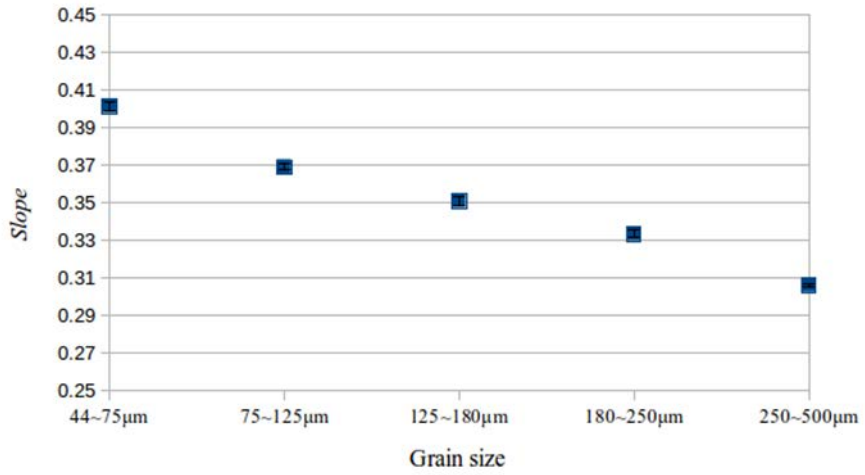

714

715 (a) Sample B

716

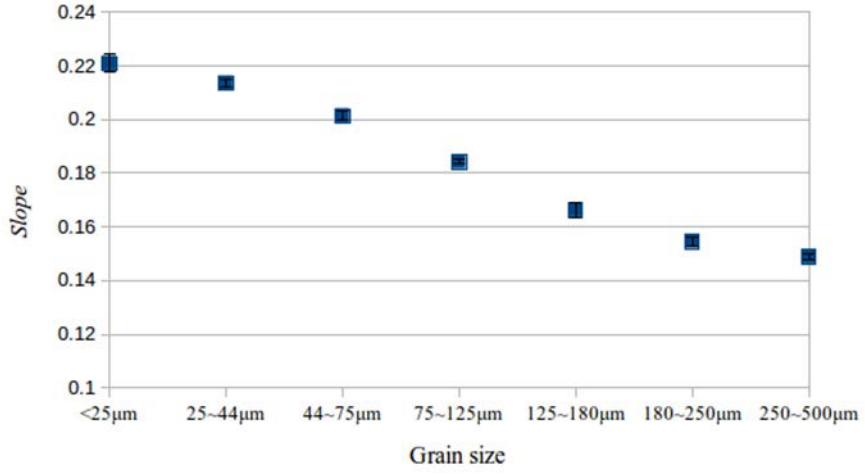

717

718 (b) Sample F

719

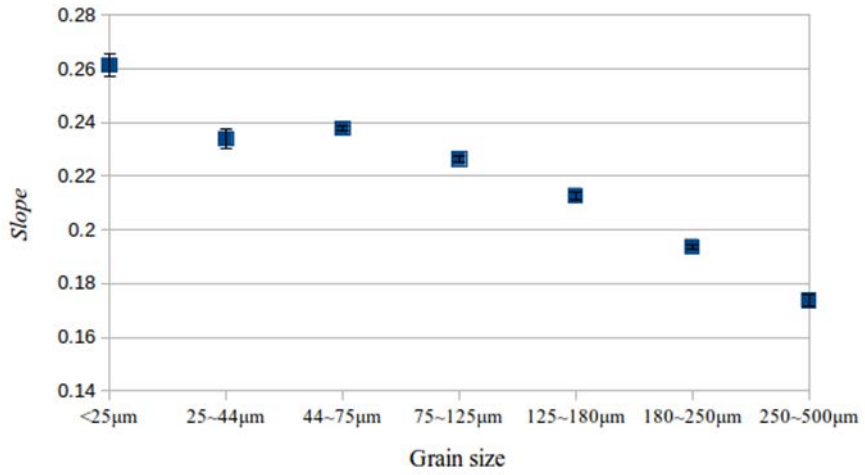

720

721 (c) Sample G

722 Figure 2. *Slope* in reflectance spectra of different grain size samples. *Slope* decreases as

723 grain size increases.

724

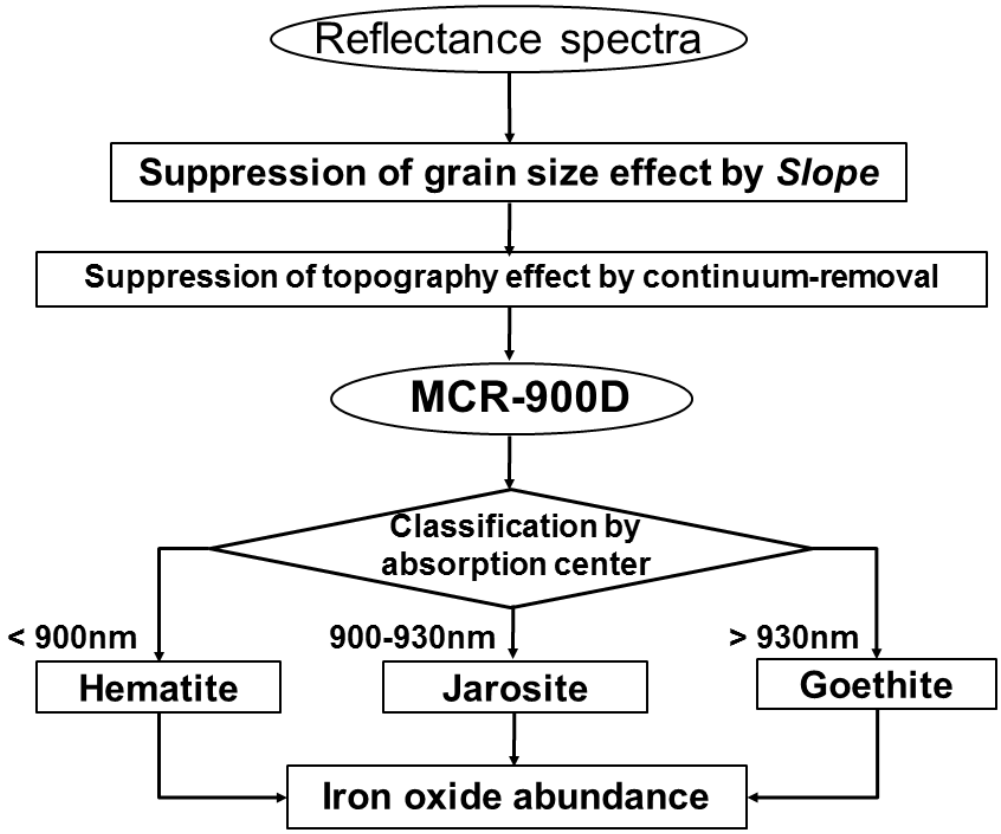

725

726

727 Figure 3. Processing sequence of the proposed method for different forms of iron oxide

728 minerals.

729

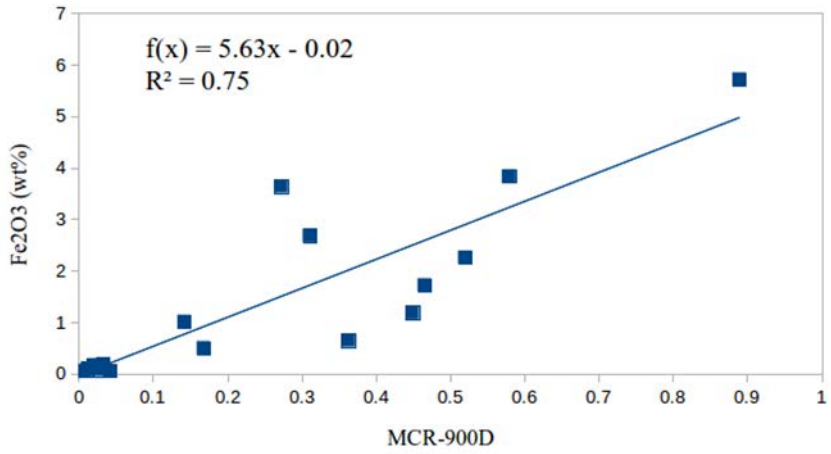

730

731 (a) Hematite samples

732

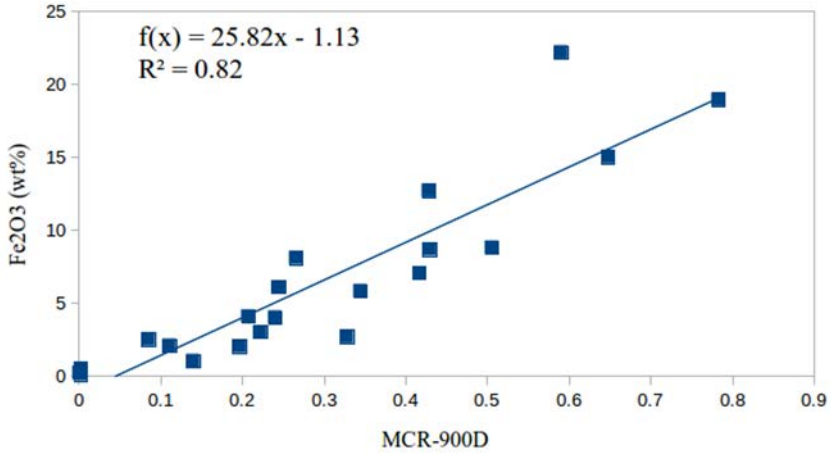

733

734 (b) Goethite samples

735

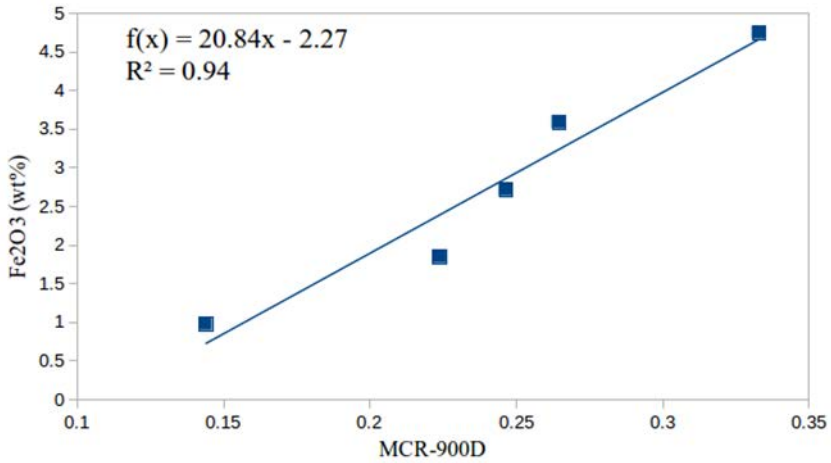

(c) Jarosite samples

Figure 4. Correlations between MCR-900D and Fe_2O_3 contents of (a) hematite (n=17), (b) goethite (n=21) and (c) jarosite (n=5) samples.

741 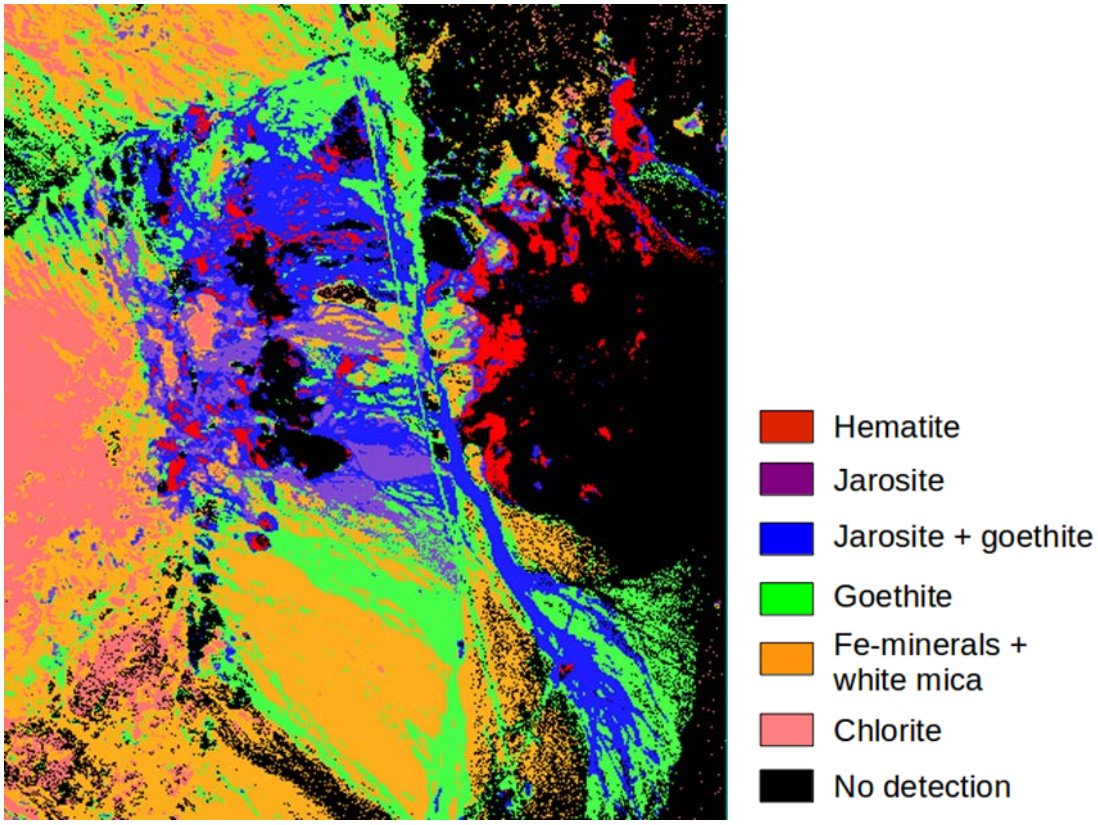

742 Figure 5. Iron oxide mineral map derived from the AVIRIS VNIR (400-1350 nm) data
743 by using the supervised maximum likelihood classifier for the area of hydrothermal
744 alteration at Cuprite in Nevada, USA.

745

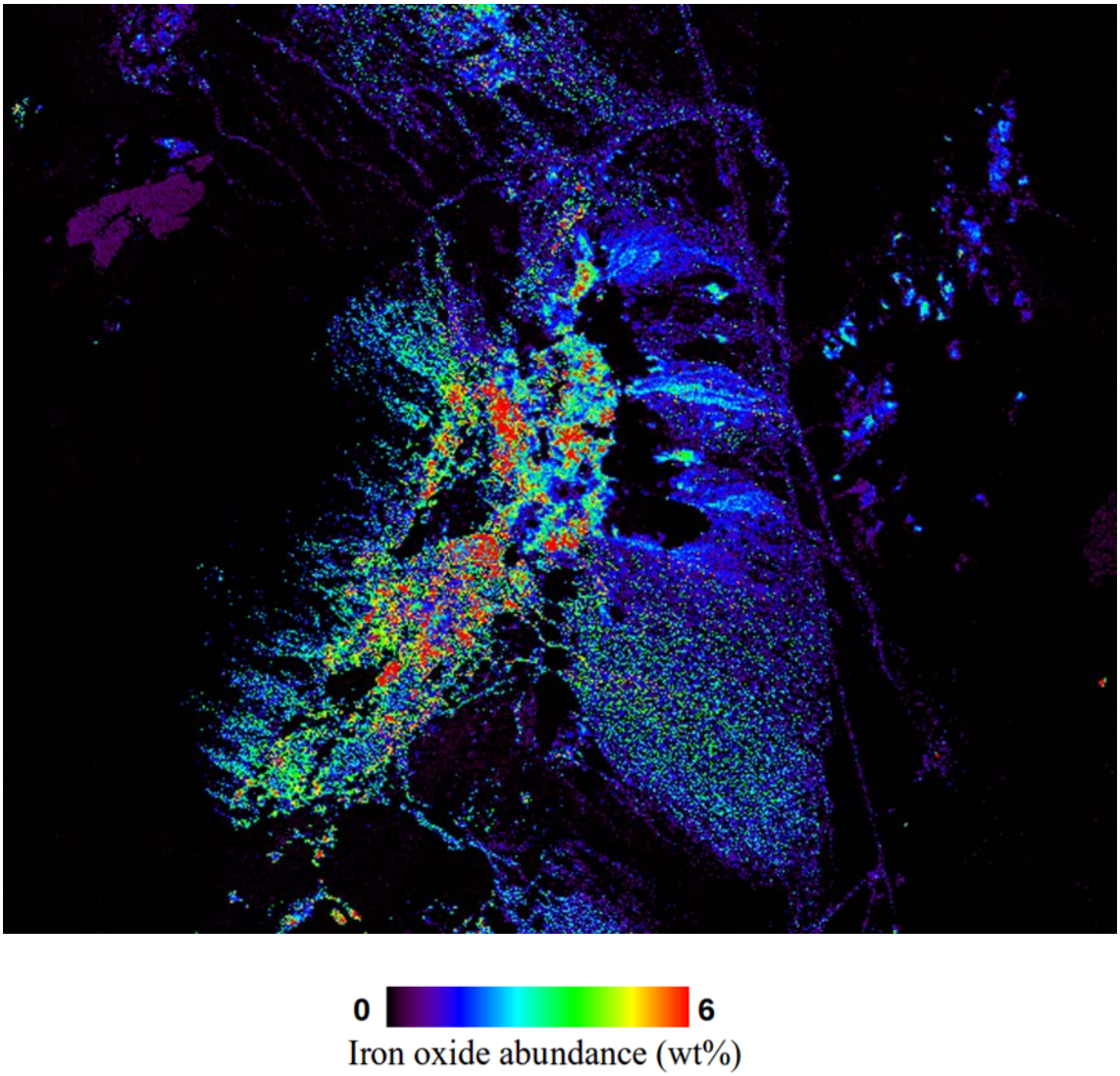

Figure 6. Iron oxide abundance map derived using MCR-900D for the Cuprite area in Nevada, USA.

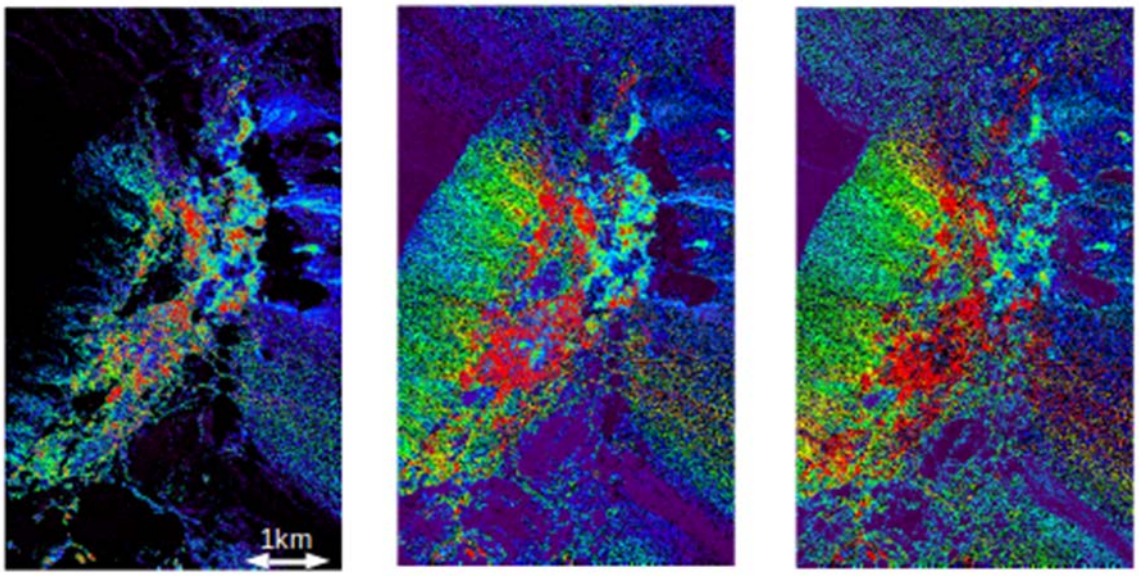

Figure 7. Iron oxide abundance map derived using each method (left: MCR-900D, middle: CR-900D, right: 900D) for the western hills in the Cuprite area in Nevada, USA.